# Clinical Feasibility of Noninvasive Visualization of Lymphatic Flow with Principles of Spin Labeling MR Imaging: Implications for Lymphedema Assessment[1]

Swati Rane, PhD
Paula M. C. Donahue, PT, DPT, CLT, MBA
Ted Towse, PhD
Sheila Ridner, BSN, MSHSA, MSN, PhD, ACNP
Michael Chappell, MEng, DPhil
John Jordi, PTA, CLT-LANA
John Gore, PhD
Manus J. Donahue, PhD

**Purpose:** To extend a commonly used noninvasive arterial spin labeling magnetic resonance (MR) imaging method for measuring blood flow to evaluate lymphatic flow.

**Materials and Methods:** All volunteers ($n = 12$) provided informed consent in accordance with institutional review board and HIPAA regulations. Quantitative relaxation time (T1 and T2) measurements were made in extracted human lymphatic fluid at 3.0 T. Guided by these parameters, an arterial spin labeling MR imaging approach was adapted to measure lymphatic flow (flow-alternating inversion-recovery lymphatic water labeling, $3 \times 3 \times 5$ mm) in healthy subjects ($n = 6$; mean age, 30 years $\pm$ 1 [standard deviation]; recruitment duration, 2 months). Lymphatic flow velocity was quantified by performing spin labeling measurements as a function of postlabeling delay time and by measuring time to peak signal intensity in axillary lymph nodes. Clinical feasibility was evaluated in patients with stage II lymphedema (three women; age range, 43–64 years) and in control subjects with unilateral cuff-induced lymphatic stenosis (one woman, two men; age range, 31–35 years).

**Results:** Mean T1 and T2 relaxation times of lymphatic fluid at 3.0 T were 3100 msec $\pm$ 160 (range, 2930–3210 msec; median, 3200 msec) and 610 msec $\pm$ 12 (range, 598–618 msec; median, 610 msec), respectively. Healthy lymphatic flow (afferent vessel to axillary node) velocity was 0.61 cm/min $\pm$ 0.13 ($n = 6$). A reduction ($P < .005$) in lymphatic flow velocity in the affected arms of patients and the affected arms of healthy subjects with manipulated cuff-induced flow reduction was observed. The ratio of unaffected to affected axilla lymphatic velocity ($1.24 \pm 0.18$) was significantly ($P < .005$) higher than the left-to-right ratio in healthy subjects ($0.91 \pm 0.18$).

**Conclusion:** This work provides a foundation for clinical investigations whereby lymphedema etiogenesis and therapies may be interrogated without exogenous agents and with clinically available imaging equipment.

© RSNA, 2013

Supplemental material: *http://radiology.rsna.org/lookup/suppl/doi:10.1148/radiol.13120145/-/DC1*

**Radiology**

Breast cancer treatment–related lymphedema is characterized by chronic incurable swelling of the arm and occasionally the trunk after axillary lymph node dissection and represents a major health concern in developed nations (1). Of approximately 2.3 million breast cancer survivors in the United States, 19%–49% of patients who undergo axillary lymph node dissection and radiation therapy develop lymphedema (2–4). Identification of subclinical lymphedema has shown that only 7% of patients who receive structured physical therapy develop lymphedema in the 1st year, relative to 25% of control subjects who do not receive physical therapy (5). Thus, early identification of patients at high risk for lymphedema is critical; however, cost-effective screening that does not require specialized equipment is required for widespread implementation (6).

Recently, lymphatic contractility and pumping have been measured by using technetium 99m nuclear imaging, which has shown that reduction in lymphatic velocity is proportional to the severity of swelling and that intersubject variability

in lymphatic pump failure may contribute to lymphedema risk (7). However, routine clinical implementation of comparable computed tomographic (CT) (8,9), optical (10), and magnetic resonance (MR) lymphangiographic (11) techniques is complicated by requirements for ionizing radiation, specialized optical probes and fluorophores, and/or exogenous contrast agents, respectively (6). Thus, radiologic screening could greatly benefit from procedures that yield comparable information but are easier to implement.

MR imaging has been widely used to evaluate fluid transportation in several contexts; however, noninvasive MR imaging techniques with which to assess lymphatic flow remain underdeveloped. Importantly, to our knowledge, even basic measurements of relaxation times of human lymphatic fluid (T1 and T2) at current imaging fields have not been published, thereby precluding rigorous quantification of lymphatic contrast. However, the principles of lymphatic flow are analogous to those of blood and cerebrospinal fluid flow, two physiologic phenomena that have been measured successfully with MR imaging for more than 2 decades (12–14). The lymphatic system is unidirectional and open ended; lymphatic fluid is carried to lymph nodes via lymphatic collectors through forces supplied by smooth muscle contractions. Thus, noninvasive arterial spin labeling MR imaging approaches commonly used to magnetically label blood water and

quantify blood flow and tissue perfusion and that have been used clinically in oncology (15), cerebrovascular disease (16–18), and cognitive neuroimaging (19,20) should translate to lymphatic imaging. The major obstacles include (a) slower velocity of lymph relative to blood and (b) increased field heterogeneity and radiofrequency (RF) labeling inefficiency in the extremities. We hypothesize that these difficulties can be alleviated (a) because of the longer lymphatic water T1 relaxation time relative to the blood water T1 relaxation time and (b) by applying new hardware advances, including multichannel receive coils in conjunction with parallel RF transmit technology, to detect and label lymphatic water over small regions with high efficiency.

The purpose of this study was to extend a commonly used noninvasive arterial spin labeling MR imaging method for measuring blood flow to evaluate lymphatic flow.

## Materials and Methods

This study was approved by the Vanderbilt University institutional review board. All patients and healthy subjects provided informed written consent. Approximately 200 mL of lymphatic fluid was acquired at three different dates and times in a 16-year-old female

---

### Advances in Knowledge

- Quantitative longitudinal (T1) and transverse (T2) relaxation time measurements of human lymphatic fluid are presented at 3.0 T.

- Feasibility of noninvasive assessment of lymphatic flow velocities by using principles of spin labeling is shown, analogous to the popular arterial spin labeling method used to quantify perfusion.

- Expected reductions in lymphatic flow velocity are found both in healthy individuals under conditions of manipulated lymphatic flow obstruction and in patients with stage II lymphedema.

- A kinetic model for lymphatic spin labeling measurements is introduced, and it can be used to quantitatively understand sources of variability in patients.

### Implication for Patient Care

- An MR imaging method capable of quantifying lymphatic flow velocities without exogenous contrast agent administration is presented; this method can be readily implemented with commercially available MR imagers and enables noninvasive assessment of lymphatic flow in vivo, which should be useful in the identification of disease biomarkers or the evaluation of therapies in patients with post–breast cancer–related lymphedema.

patient with a congenital deep lymphatic impairment that required an abdominal lymphatic shunt to permit self-drainage of lymphatic fluid collection. The fluid was immediately transferred to a sterile container, deidentified, maintained at physiologic temperature, and transported to the imaging facility. Because the lymph sample typically would have been discarded as waste and because this sample was deidentified before it was brought to the imaging institute, the institutional review board determined this aspect of the study did not qualify as human subject research. The study was in compliance with Health Insurance Portability and Accountability Act regulations.

### Relaxation Time Measurements

Lymphatic fluid experiments were conducted within approximately 30 minutes of fluid extraction with a Philips 3.0-T MR imager (Achieva; Philips Medical Systems, Best, the Netherlands). The fluid sample was maintained at body temperature by using a warm water bath throughout imaging. A thermochromic thermometer (Apothecary Products, Minneapolis, Minn) was used to monitor sample temperature.

*T1 measurement.*—Images were acquired at different inversion times (range, 0–10 000 msec at an interval of 500 msec), as well as with a long inversion time (20 sec) for equilibrium magnetization calibration. Other parameters were as follows: repetition time msec/echo time msec, 40 000/28; spatial resolution, $3 \times 3 \times 5$ mm; and single-shot echo-planar imaging, with 16-msec hyperbolic secant adiabatic inversion prepulse. Inversion pulse duration and $B_1$ were optimized for efficiency prior to T1 measurements. T1 was calculated by using a three-point fit of the magnitude signal ($S$) and the equation

$$S(\mathrm{TI}) = \left| S_0 \left\{ 1 + \left[ \cos(\theta) - 1 \right] \cdot e^{-\mathrm{TI/T1}} \right\} \right| \quad [1],$$

where $S_0$ is the equilibrium signal intensity, $S(\mathrm{TI})$ is the magnitude signal intensity, TI is the inversion time, and $\theta$ is the inversion angle. To confirm that T1

of the lymphatic fluid samples was representative of lymphatic water T1 in the axilla, an inversion recovery experiment was performed in a healthy volunteer. We chose the inversion time such that $M_z(\mathrm{TI})/M_0 = (1 - 2e^{-\mathrm{TI/T1}} + e^{-\mathrm{TR/T1}}) = 0$, where $M_z$ is the longitudinal magnetization along the z axis, $M_0$ is the steady state magnetization, T1 was measured lymphatic water T1, and repetition time was 4 seconds. Signal-to-noise ratio measurements were made for images with (denoted as *nulled*) and without (denoted as *not nulled*) the inversion prepulse and were compared with measurements in a free-form region of noise (160 voxels) within the surrounding lung cavity. Thus, this is similar to a fluid-attenuated inversion recovery experiment but with the inversion time chosen to correspond to the presumed lymphatic water $M_z$ null point rather than the cerebrospinal fluid $M_z$ null point.

*T2 measurement.*—Eight images, each obtained with a different echo time, were acquired with a multiecho spin-echo echo-planar imaging sequence. Data were oversampled during the period of maximal signal decay, yielding echo time points at 50, 150, 250, 350, 600, 1000, and 1400 msec. Other parameters included repetition time of 2500 msec and spatial resolution of $3 \times 3 \times 5$ mm. T2 was quantified by using the monoexponential equation:

$$S = S_0 e^{-\mathrm{TE/T2}} \quad [2].$$

For the first sample, the range of echo times was still under optimization and was too low (0–200 msec) to enable accurate T2 measurement. Thus, only the second and third samples were used for T2 calculations.

### Spin Labeling Measurements in Unobstructed Lymphatic System

The idea for spin labeling MR imaging is to acquire two sets of images, one with and one without magnetic labeling of inflowing water. After the labeling prepulse, an inversion time is allowed (generally 1–2 sec), which describes the amount of time after labeling and before acquisition. By comparing the

difference in image contrast between labeled and unlabeled images, a flow-weighted image can be obtained. For perfusion, the difference in image signal is small at only 1%–2% of tissue signal; this signal arises from the small amount of perfusion-weighted contrast relative to total signal intensity and the decay of the magnetic label with blood water T1. For 3.0-T blood water, T1 is approximately 1600 msec (21); however, a longer T1 would increase signal-to-noise ratio and enable spin labeling to be performed for low-velocity scenarios.

Experiments were performed in healthy subjects at 3.0 T ($n = 6$; two men, four women; mean age, 30 years $\pm$ 1). To accurately identify the location of axillary nodes, a diffusion-weighted inversion with background suppression (DWIBS) examination was used (spatial resolution, $3 \times 3 \times 5$ mm; *b* value, 800 sec/mm$^2$; repetition time msec/ echo time msec/inversion time msec, 8037/49.79/260), which shows high contrast between lymph nodes and surrounding tissue. For all acquisitions, a dual-channel (parallel $B_1$) body coil and a 16-channel torso coil were used for RF transmission and reception, respectively. Next, a spin labeling approach with the same section geometry and an alternating section-selective and nonselective (22) hypersecant 11-msec inversion prepulse was used, followed by an inversion time range of 500 to 8000 msec in 500-msec increments, to quantify transit time (23). The previously described pulsed spin labeling approach was chosen in favor of pseudocontinuous labeling owing to the low velocity of lymphatic fluid and the difficulty of meeting flow-driven inversion criteria with high efficiency (24). A spectral presaturation with inversion recovery prepulse that was frequency selective for fat was used (7.5 msec; bandwidth, 190 Hz) for optimized fat suppression immediately before the RF excitation for section acquisition. Other imaging parameters were as follows: echo time, 4 msec; spatial resolution, $3 \times 3 \times 5$ mm; sensitivity encoding factor, two; half scan factor, 0.6; nine signals acquired; and single-shot gradient-echo echo-planar imaging.

Flow-weighted maps were obtained by subtracting the nonselective inversion image from the section selective inversion in pairwise fashion ($\Delta M$) and normalizing by equilibrium magnetization ($M_0$). $M_0$ was calculated by using an inversion recovery image from the longest inversion time point. The DWIBS image was used to identify the location of the axillary lymph nodes for the subsequent spin labeling experiment. Finally, with the adiabatic inversion pulse used here, we experimentally determined that the RF spillover/spatial tagging inefficiency was approximately 0.5 mm or 10% of the section thickness. Thus, the lymph velocity entering the node is estimated according to 0.5 mm divided by time to peak. Reproducibility, interrater variability, and motion were also assessed and are addressed in Appendixes E1 and E2 (online).

### Spin Labeling Measurements in Obstructed Lymphatic System

Importantly, the lack of a reference standard for lymphatic imaging precludes a clear method for validating the lymphatic spin labeling measurements. Thus, we performed additional ($n = 6$) measurements with known asymmetric lymphatic impairment. This included measurements in three healthy subjects (two men and one woman 31, 31, and 35 years, respectively) with a unilateral blood pressure cuff and clinical feasibility assessment in three female patients (aged 60, 43, and 64 years) with stage II lymphedema secondary to unilateral breast mastectomy and radiation therapy. The ages of these groups were not matched, as the purpose of this experiment was not to specifically compare groups but rather to demonstrate asymmetric lymphatic velocity under varying conditions of known lymphatic impairment. Additionally, this component of the study was simply to determine if altered lymphatic flow properties could be detected under conditions of obstructed lymphatic flow, rather than to provide a detailed description of the range of lymphatic obstruction in patients, which would require additional imaging data. All patients volunteered to participate in

research by responding to research flyers posted at a local lymphedema clinic and were more than 6 months removed from their most recent radiation treatment. To simulate impaired flow conditions, lymphatic flow was obstructed in the left arm of the right-handed healthy subjects by using a blood pressure cuff, with pressure maintained at 60 mmHg. Note that as the cuff was applied unilaterally and all patients had unilateral lymph node dissection, the contralateral (unaffected) side was used as an internal control in all subjects. Diastolic blood pressure in the healthy subjects ranged from 66 to 75 mmHg, which enabled us to confirm that venous occlusion would not occur (7). To allow for reduced flow scenarios in both the cuffed healthy subjects and the patients, sampling was performed over a broader range of potential inflow times (3500–10 000 msec) sampled in 500-msec increments. To reduce the overall examination duration, the number of signals acquired was decreased to eight, leading to a total duration of approximately 40 minutes. Specifically for the impaired flow study, data with short labeling delays (500–1500 msec) were not acquired, since measuring blood flow was not the intent of these experiments and extending the postlabeling delay range in such a manner would have added considerably to the total examination time. This approach enabled us to measure the longer transit times and slow velocities of the obstructed lymph within a time feasible for a study in the clinic.

Since the sample sizes in this feasibility report are small, nonparametric testing was performed to assess significance of measured velocity differences in the unaffected versus affected (stage II lymphedema or cuff-obstructed flow) arms, as well as in the ratio of the affected-to-unaffected lymph-to-axilla velocity of patients versus left-to-right lymph-to-axilla velocity in healthy subjects. Significance of the measurements was evaluated by using the Wilcoxon signed rank test available within the Matlab software (Mathworks, Natick, Mass). The criterion for a significant difference was $P < .05$.

## Results

### Relaxation Time Results

Figure 1 shows a representative inversion recovery curve obtained from a lymphatic fluid sample from which T1 was calculated, as well as the signal intensity decay of the same sample as a function of echo time from which T2 was calculated. Mean T1 and T2 of lymphatic fluid at 3.0 T were found to be 3100 msec $\pm$ 160 (individual measurements: 3210, 3200, and 2930 msec) and 610 msec $\pm$ 12 (individual measurements, 616 and 598 msec), respectively. When an inversion recovery acquisition was performed in vivo on a test subject to null the lymphatic signal with this T1 value, lymph node signal was reduced by a factor of 3.3 (nulled vs not nulled, 6 arbirary units [AU] $\pm$ 3 vs 20 AU $\pm$ 8) and was not significantly different ($P = .29$) from the noise signal (4 AU $\pm$ 2).

### Spin Labeling Measurements in Unobstructed Lymphatic System

Figure 2 shows an example DWIBS image with a corresponding control spin labeling image. The lymph nodes, which were identified on the DWIBS image, were overlaid on the echo-planar image from the spin labeling examination for clarity, and free-form regions of interest in the lymph nodes (two to four voxels) and a major artery (three to five voxels) were drawn (S. Rane, M.J.D.; 7 and 11 years of MR experience, respectively). An experienced radiologist was consulted to verify and confirm that the regions of interest drawn based on the DWIBS image correctly colocalized with the lymph nodes. Mean changes in the spin labeling signal ($\Delta M/M_0$) from the blood and axillary lymph nodes are shown in Figure 3. In all subjects, contrast in the blood increases quickly owing to the fast passage of blood through the large artery, whereas the curve in the lymph node rises later owing to the much slower velocity of lymphatic fluid. Note that because of the comparatively short T1 of blood water (approximately 1600–1700 msec at 3.0 T), it was not possible for this signal change to arise

Radiology
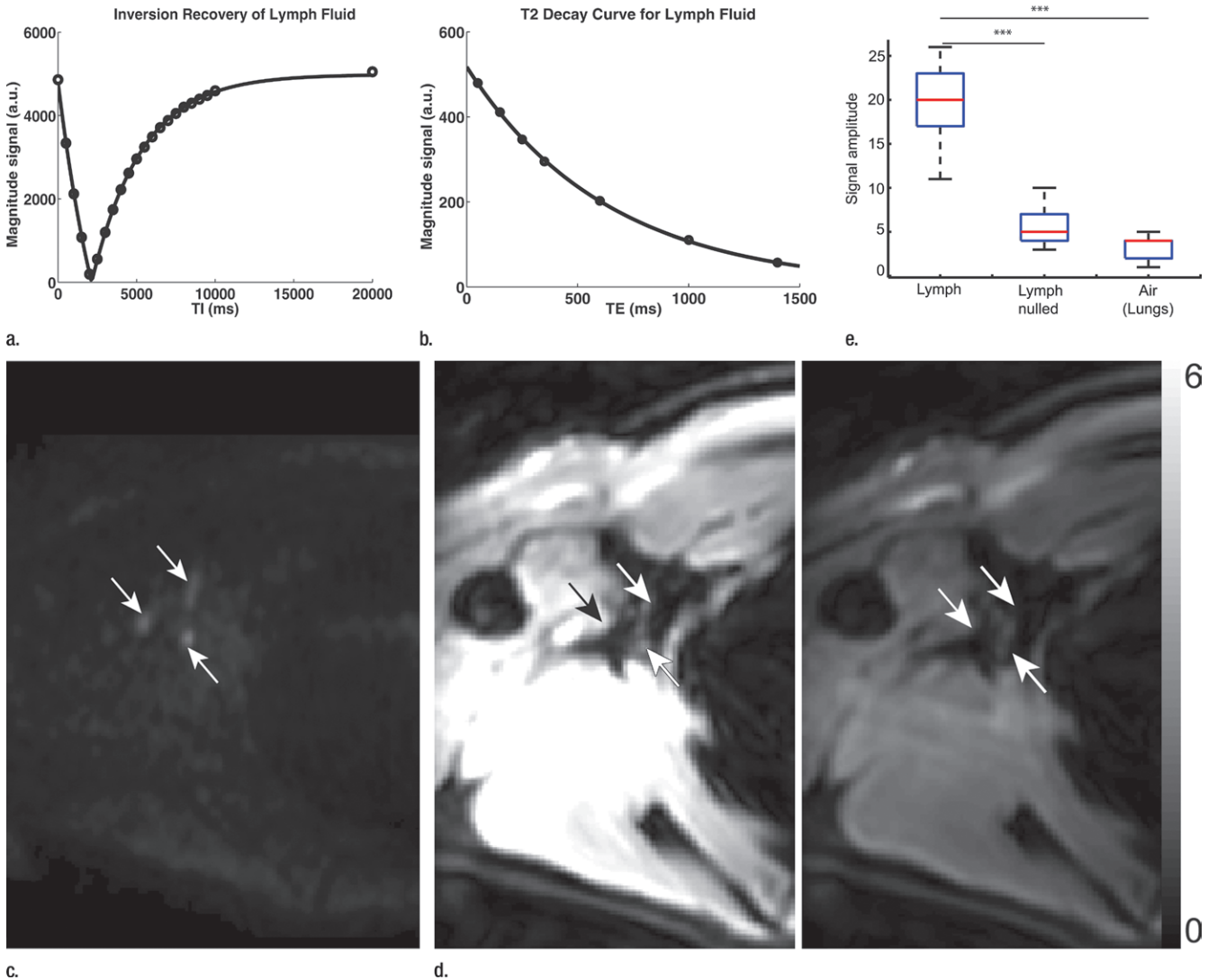
### Figure 1



**Figure 1:** Relaxation time measurements. Graphs of **(a)** inversion recovery and **(b)** exponential spin-echo decay of a representative lymphatic fluid sample at 38°C. Experimental data (●) and fit (solid line) are shown (Equations 1 and 2, respectively). **(c, d)** In vivo MR images of lymph nodes (arrows) acquired with **(c)** DWIBS and **(d)** without (left) and with (right) inversion prepulse with echo-planar imaging. Inversion prepulse was placed at the expected null point (inversion time, 1.4 sec; repetition time, 4 sec) of lymphatic water, calculated with T1 of 3100 msec measured from the ex vivo lymphatic sample. **(e)** Quantitative analysis of signal in the nodes shows that signal intensity after longitudinal nulling is not significantly different from noise signal. This provides support for the ex vivo T1 measurements reflecting in vivo lymphatic water T1. Red line represents the median, while the box represents the 25th and 75th percentiles. Error bars indicate the most extreme values in the data. *** = $P < .001$.

from blood water. The transit time for lymph water was 5100 msec ± 970 (median, 5500 msec; range, 3500–6000 msec), and the time to peak was 5800 msec ± 880 (median, 6250 msec; range, 4500–6500 msec), which leads to a calculated lymphatic fluid velocity at the level of the afferent vessel entering the node of 0.61 cm/min ± 0.13 (median, 0.57 cm/min; range, 0.5–0.85 cm/min).

### Spin Labeling Measurements in Obstructed Lymphatic System

There was a reduction in lymphatic flow velocity in the affected (mean, 0.48 cm/min ± 0.15; median, 0.46 cm/min; range, 0.33–0.66 cm/min) versus unaffected (mean, 0.61 cm/min ± 0.22; median, 0.58 cm/min; range, 0.35–0.85 cm/min) arms of patients with stage II lymphedema ($P = .06$) and in the affected (mean, 0.47 cm/min ± 0.14; median, 0.46 cm/min; range, 0.31–0.66 cm/min) versus unaffected (mean, 0.58 cm/min ± 0.16; median, 0.66 cm/min; range, 0.35–0.75 cm/
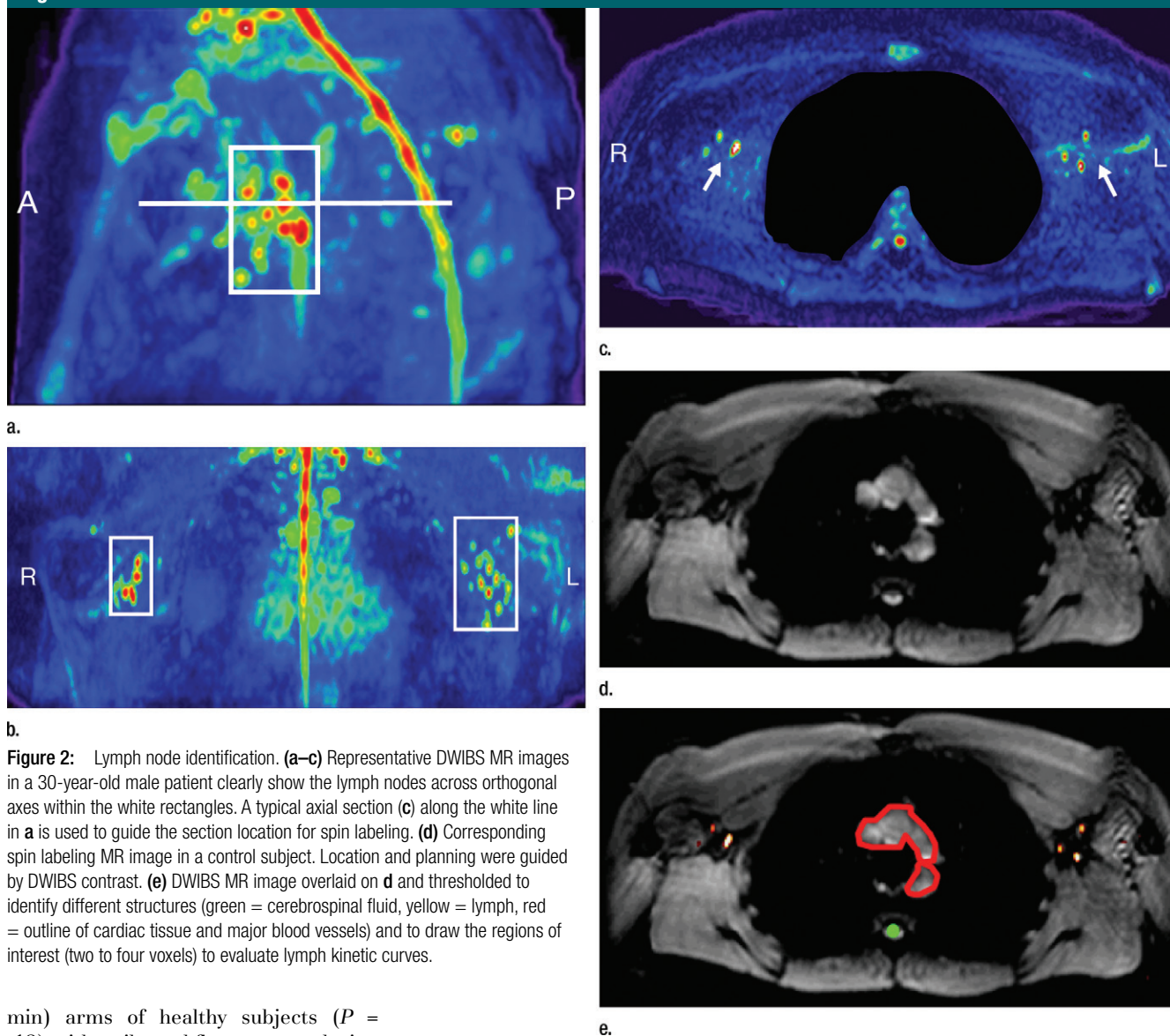
Figure 2

a.

b.

c.

d.

e.

**Figure 2:** Lymph node identification. **(a–c)** Representative DWIBS MR images in a 30-year-old male patient clearly show the lymph nodes across orthogonal axes within the white rectangles. A typical axial section (**c**) along the white line in **a** is used to guide the section location for spin labeling. **(d)** Corresponding spin labeling MR image in a control subject. Location and planning were guided by DWIBS contrast. **(e)** DWIBS MR image overlaid on **d** and thresholded to identify different structures (green = cerebrospinal fluid, yellow = lymph, red = outline of cardiac tissue and major blood vessels) and to draw the regions of interest (two to four voxels) to evaluate lymph kinetic curves.

min) arms of healthy subjects ($P$ = .12) with unilateral flow stenoocclusion when a pressure cuff was used (Fig 4). When the groups of three subjects were compared for asymmetric delay in lymphatic velocity, the differences were not significant ($P$ = .06–.12); however, they became significant ($P$ = .004) when the two groups were considered together (Fig 4b). Unaffected-to-affected ratio was 1.27 ± 0.18 in patients with stage II lymphedema and 1.21 ± 0.18 in healthy subjects with cuff-obstructed flow; left-to-right ratio was 0.91 ± 0.08 in healthy subjects with unobstructed flow.

## Discussion

The overall finding of this work is that long T1 of lymphatic water enables us to estimate lymphatic velocity with spin labeling methods. Clinical feasibility of this approach is also demonstrated in patients with lymphatic flow obstruction.

Our measurements of T1 and T2 values for human lymph at 3.0 T should be useful to generate optimized lymphatic MR imaging contrast. These measurements have not been performed in the past because of the difficulty of isolating the pure lymphatic voxels in vivo and the pure lymphatic fluid samples ex vivo. Similar to blood water T1, which varies with oxygenation and hematocrit level, lymphatic T1 will vary with location, protein content, and disease severity. The ex vivo T1 measurement was approximately correct in in vivo $M_z$ nulling experiments. Finally, it should be noted that blood water additionally varies with oxygenation, vessel size, and hematocrit level; thus, the success
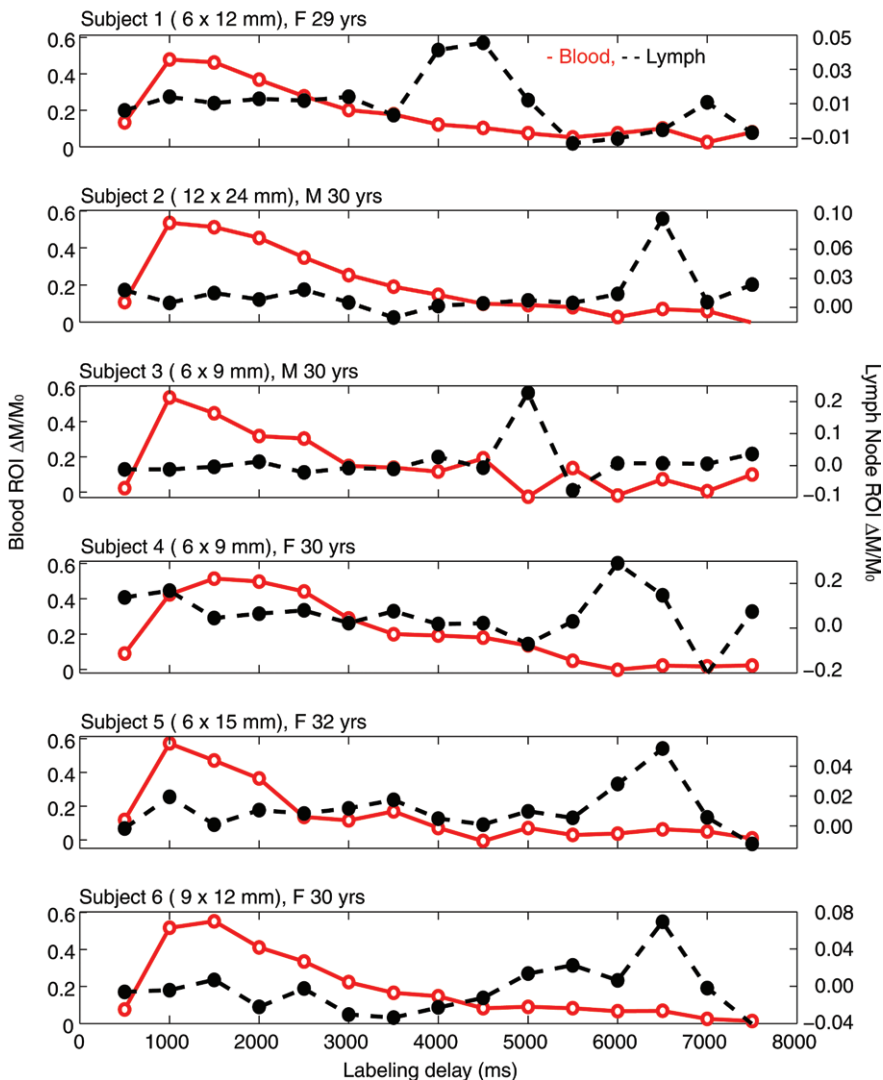
### Figure 3



**Figure 3:** Unobstructed lymphatic flow results. Lymphatic and blood water magnetization as a function of postlabeling delay times in six separate healthy subjects. In-plane dimensions of lymph nodes evaluated for each subject are also reported. Note that blood signal increases quickly owing to the short T1 of blood water and fast blood water velocity. Alternatively, signal in the axillary lymph node increases much later, because of the much slower velocity of lymph fluid. The relatively rapid rise and fall of the lymphatic curve is consistent with mixing of lymphatic water in the node and finite node dwell times, similar to the macrovascular blood compartment in arterial spin labeling experiments (Appendix E3 [online]). *F* = female, *M* = male, *ROI* = region of interest.

of arterial spin labeling may be interpreted as an exemplar for why small variations in lymphatic T1 may not be an overwhelming confounding variable.

In the context of literature values, the velocity measured in our study is slower than that in most studies that measured large-vessel velocity.

Importantly, to phagocytose and filter detrimental substances, lymph flow into the intranodal sinus system is much slower than in large vessels populated with lymphangions (25). Additionally, as lymph circulates through multiple nodes, it becomes denser and reduces velocity. By using technetium 99m

human immunoglobulin G, Modi et al (7) found a relatively large mean hand-to–axillary node velocity of 8.9 cm/min ± 5.8, with a transit time of 9.6 minutes ± 7.2. By using fluorescence video microscopy in the foot, Fischer et al (26) showed that the median resting capillary velocity was 0.058 cm/min in the human skin. With fluorescence recovery after photobleaching in a mouse model, Berk et al (27), and Swartz et al (28) found the velocity to be 0.028 cm/min and 0.018–0.024 cm/min, respectively. Most studies are performed in superficial lymphatic vessels and are performed over short distances with invasive dyes that change vessel pressure and skin lymphatic activity. The mean entry velocity measured here (0.61 cm/min) is on the lower end of the reported velocity ranges for large and small vessels, as expected for the location of the measurement. Other MR approaches have also been used with some success to detect lymph nodes and evaluate lymphatic flow by using ultrasmall superparamagnetic iron oxide and gadolinium chelates, albeit with low sensitivity (6). A study (29) to assess the reproducibility, reliability, and accuracy of unenhanced MR imaging methods, specifically T1-weighted imaging and diffusion-weighted imaging (30), in metastatic lymph nodes in patients with breast cancer concluded that these methods are not yet ready for clinical implementation. However, promising work in animals has shown that very-low-dose gadolinium-conjugated dendrimers, which have been used successfully in pigs, potentially could be used in humans (31).

Our findings in controlled pressure cuff scenarios in healthy subjects and patients with intermediate-stage (stage II) lymphedema showed reduced lymphatic velocity in the affected arm. The number of subjects who were studied for obstructed lymph flow measurements was low, since the primary purpose of the study was to assess feasibility. The lymphatic velocity, although frequently reduced, showed a trend for a significant reduction in the affected versus unaffected arms in both groups. Importantly, combining the two
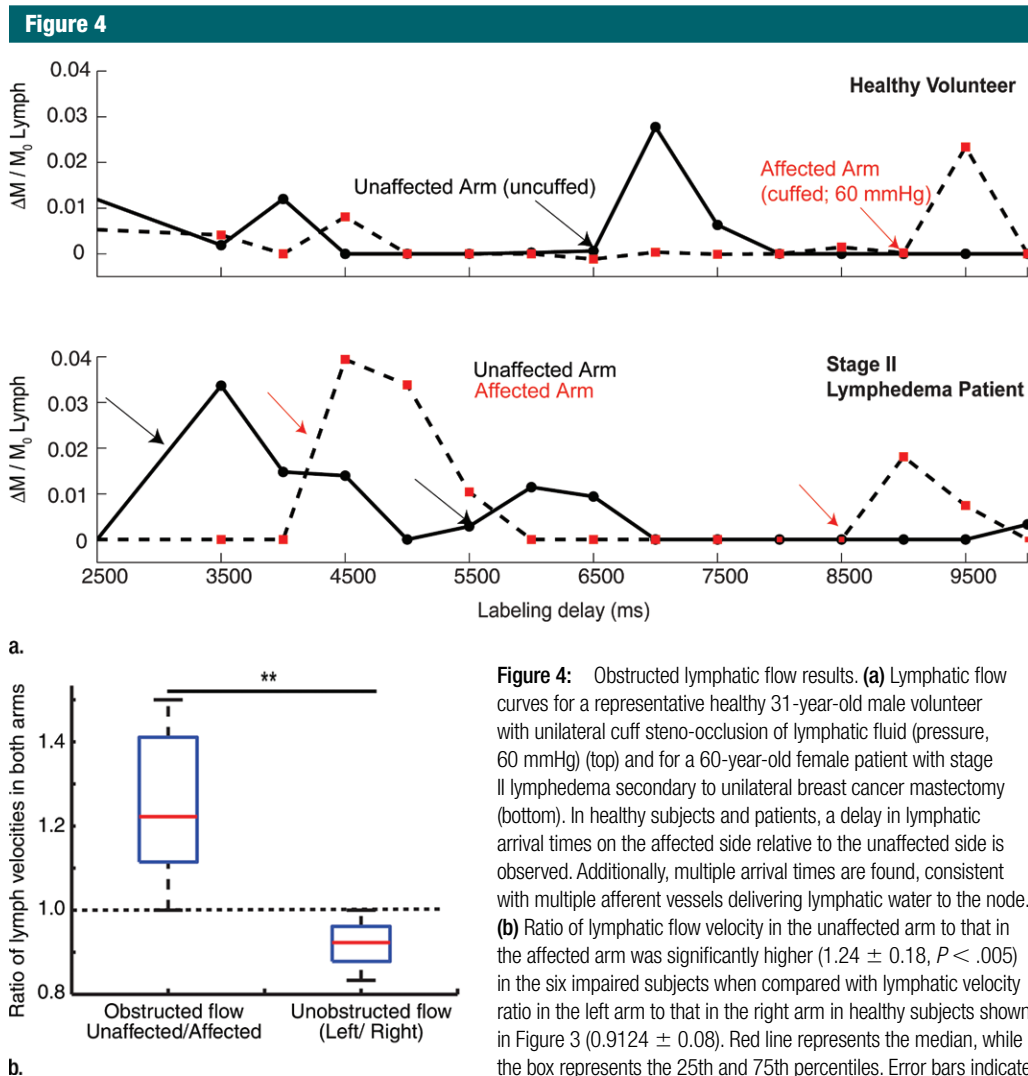
## Figure 4



**Figure 4:** Obstructed lymphatic flow results. **(a)** Lymphatic flow curves for a representative healthy 31-year-old male volunteer with unilateral cuff steno-occlusion of lymphatic fluid (pressure, 60 mmHg) (top) and for a 60-year-old female patient with stage II lymphedema secondary to unilateral breast cancer mastectomy (bottom). In healthy subjects and patients, a delay in lymphatic arrival times on the affected side relative to the unaffected side is observed. Additionally, multiple arrival times are found, consistent with multiple afferent vessels delivering lymphatic water to the node. **(b)** Ratio of lymphatic flow velocity in the unaffected arm to that in the affected arm was significantly higher ($1.24 \pm 0.18$, $P < .005$) in the six impaired subjects when compared with lymphatic velocity ratio in the left arm to that in the right arm in healthy subjects shown in Figure 3 ($0.9124 \pm 0.08$). Red line represents the median, while the box represents the 25th and 75th percentiles. Error bars indicate the extreme values measured in this data. Dashed line represents the line of unity indicating identical lymph velocity in both arms. ∗∗ = $P < .005$.

populations resulted in a significant ($P < .005$) decrease in lymphatic velocity on the impaired side when compared with the unimpaired side. Furthermore, the ratio of lymphatic velocity in the unaffected arm to lymphatic velocity in the affected arm is significantly ($P < .005$) greater than the ratio of lymphatic flow velocities in both arms in healthy subjects, which is approximately one, indicating identical lymph flow in the healthy left and right arms. This outcome supports the idea that the lymphatic spin labeling technique can

be used to detect clinical differences in lymphatic flow velocity.

Additionally, it should be noted that the rise and fall of the lymphatic spin labeling kinetic curve is much sharper than that of the perfusion kinetic curve. We have outlined a kinetic model justifying this response in Appendix E3 (online) and believe that this effect occurs because the lymphatic system more closely reflects the macrovascular compartment of arterial spin labeling models, with the addition of mixing within the node and an extended dwell time.

Several limitations of this study should be considered. First, our approach measures lymph flow into the nodes and does not discriminate between how many nodes the fluid has traversed, which will influence viscosity and velocity. However, in cases of obstructed flow, we did observe differences in affected versus unaffected arms, lending support to the clinical potential of this technique. Lymphatic velocity will likely be much slower in patients with lymphedema, causing the spin labeling curves to shift further to the right. This

may cause the lymphatic water label to decay before it enters the node. However, the T1 of lymphatic water is very long at 3.0 T (3100 msec). Thus, for efficient RF inversion pulses, longitudinal magnetization will be reduced from equilibrium by approximately 29% (at a time to peak of 6000 msec) to approximately 8% (at a time to peak of 10 000 msec). Efficient spin labeling does allow for flow estimation over a large time-to-peak range, as shown in the clinical feasibility test. Multisection approaches could be implemented, enabling lymph flow measurements over a larger spatial domain. Finally, signal-to-noise ratio can be increased through background suppression pulses, whereby the static signal within a section is suppressed by using principles of inversion recovery (32). Background suppression, in potential combination with other spin labeling improvement variants, such as magnetization transfer, steady-state free precession, or diffusion gradients, may additionally help better identify lymphatic vessels from surrounding tissue (18,33).

In conclusion, we have shown that owing to the long T1 of lymphatic fluid, principles of spin labeling can be extended to measure lymphatic flow in healthy subjects and patients with lymphedema. This approach is noninvasive, can be performed with clinically available MR imaging equipment, and holds potential in the identification of patients at highest risk for lymphedema related to breast cancer treatment or in the evaluation of response of the lymphatic system to novel therapies.

### References

1. Moseley AL, Carati CJ, Piller NB. A systematic review of common conservative therapies for arm lymphoedema secondary to breast cancer treatment. Ann Oncol 2007;18(4):639–646.

2. Armer J, Fu MR, Wainstock JM, Zagar E, Jacobs LK. Lymphedema following breast cancer treatment, including sentinel lymph node biopsy. Lymphology 2004;37(2):73–91.

3. Langer I, Guller U, Berclaz G, et al. Morbidity of sentinel lymph node biopsy (SLN) alone versus SLN and completion axillary lymph node dissection after breast cancer surgery: a prospective Swiss multicenter study on 659 patients. Ann Surg 2007;245(3):452–461.

4. Warren AG, Brorson H, Borud LJ, Slavin SA. Lymphedema: a comprehensive review. Ann Plast Surg 2007;59(4):464–472.

5. Torres Lacomba M, Yuste Sánchez MJ, Zapico Goñi A, et al. Effectiveness of early physiotherapy to prevent lymphoedema after surgery for breast cancer: randomised, single blinded, clinical trial. BMJ 2010;340:b5396.

6. Lucarelli RT, Ogawa M, Kosaka N, Turkbey B, Kobayashi H, Choyke PL. New approaches to lymphatic imaging. Lymphat Res Biol 2009;7(4):205–214.

7. Modi S, Stanton AW, Svensson WE, Peters AM, Mortimer PS, Levick JR. Human lymphatic pumping measured in healthy and lymphoedematous arms by lymphatic congestion lymphoscintigraphy. J Physiol 2007;583(Pt 1):271–285.

8. Luciani A, Itti E, Rahmouni A, Meignan M, Clement O. Lymph node imaging: basic principles. Eur J Radiol 2006;58(3):338–344.

9. Barrett T, Choyke PL, Kobayashi H. Imaging of the lymphatic system: new horizons. Contrast Media Mol Imaging 2006;1(6):230–245.

10. Hama Y, Koyama Y, Urano Y, Choyke PL, Kobayashi H. Two-color lymphatic mapping using Ig-conjugated near infrared optical probes. J Invest Dermatol 2007;127(10):2351–2356.

11. Kobayashi H, Kawamoto S, Bernardo M, Brechbiel MW, Knopp MV, Choyke PL. Delivery of gadolinium-labeled nanoparticles to the sentinel lymph node: comparison of the sentinel node visualization and estimations of intra-nodal gadolinium concentration by the magnetic resonance imaging. J Control Release 2006;111(3):343–351.

12. Detre JA, Leigh JS, Williams DS, Koretsky AP. Perfusion imaging. Magn Reson Med 1992;23(1):37–45.

13. Rosen BR, Belliveau JW, Aronen HJ, et al. Susceptibility contrast imaging of cerebral blood volume: human experience. Magn Reson Med 1991;22(2):293–299; discussion 300–303.

14. Rudin M, Sauter A. Noninvasive determination of regional cerebral blood flow in rats using dynamic imaging with Gd(DTPA). Magn Reson Med 1991;22(1):32–46.

15. Tourdias T, Rodrigo S, Oppenheim C, et al. Pulsed arterial spin labeling applications in brain tumors: practical review. J Neuroradiol 2008;35(2):79–89.

16. Bokkers RP, van der Worp HB, Mali WP, Hendrikse J. Noninvasive MR imaging of cerebral perfusion in patients with a carotid artery stenosis. Neurology 2009;73(11):869–875.

17. Detre JA, Samuels OB, Alsop DC, Gonzalez-At JB, Kasner SE, Raps EC. Noninvasive magnetic resonance imaging evaluation of cerebral blood flow with acetazolamide challenge in patients with cerebrovascular stenosis. J Magn Reson Imaging 1999;10(5):870–875.

18. Donahue MJ, Strother MK, Hendrikse J. Novel MRI approaches for assessing cerebral hemodynamics in ischemic cerebrovascular disease. Stroke 2012;43(3):903–915.

19. Pfefferbaum A, Chanraud S, Pitel AL, et al. Cerebral blood flow in posterior cortical nodes of the default mode network decreases with task engagement but remains higher than in most brain regions. Cereb Cortex 2011;21(1):233–244.

20. Donahue MJ, Blicher JU, Østergaard L, et al. Cerebral blood flow, blood volume, and oxygen metabolism dynamics in human visual and motor cortex as measured by whole-brain multi-modal magnetic resonance imaging. J Cereb Blood Flow Metab 2009;29(11):1856–1866.

21. Lu H, Clingman C, Golay X, van Zijl PC. Determining the longitudinal relaxation time (T1) of blood at 3.0 Tesla. Magn Reson Med 2004;52(3):679–682.

22. Wong EC, Buxton RB, Frank LR. Implementation of quantitative perfusion imaging techniques for functional brain mapping using pulsed arterial spin labeling. NMR Biomed 1997;10(4-5):237–249.

23. Buxton RB. Quantifying CBF with arterial spin labeling. J Magn Reson Imaging 2005;22(6):723–726.

24. Dai W, Garcia D, de Bazelaire C, Alsop DC. Continuous flow-driven inversion for arterial spin labeling using pulsed radio frequency and gradient fields. Magn Reson Med 2008;60(6):1488–1497.

25. Zuther JE. Lymphedema management: the comprehensive guide for practitioners. 2nd ed. Stuttgart, Germany: Thieme, 2009.

26. Fischer M, Franzeck UK, Herrig I, et al. Flow velocity of single lymphatic capillaries in human skin. Am J Physiol 1996;270(1 Pt 2):H358–H363.

27. Berk DA, Swartz MA, Leu AJ, Jain RK. Transport in lymphatic capillaries. II. Microscopic velocity measurement with fluorescence photobleaching. Am J Physiol 1996;270(1 Pt 2):H330–H337.

28. Swartz MA, Berk DA, Jain RK. Transport in lymphatic capillaries. I. Macroscopic measurements using residence time distribution theory. Am J Physiol 1996;270(1 Pt 2):H324–H329.

29. Scaranelo AM, Eiada R, Jacks LM, Kulkarni SR, Crystal P. Accuracy of unenhanced MR imaging in the detection of axillary lymph node metastasis: study of reproducibility and reliability. Radiology 2012;262(2):425–434.

30. Demetris AJ, Seaberg EC, Batts KP, et al. Reliability and predictive value of the National Institute of Diabetes and Digestive and Kidney Diseases Liver Transplantation Database nomenclature and grading system for cellular rejection of liver allografts. Hepatology 1995;21(2):408–416.

31. Sena LM, Fishman SJ, Jenkins KJ, et al. Magnetic resonance lymphangiography with a nano-sized gadolinium-labeled dendrimer in small and large animal models. Nanomedicine (Lond) 2010;5(8):1183–1191.

32. Ye FQ, Frank JA, Weinberger DR, McLaughlin AC. Noise reduction in 3D perfusion imaging by attenuating the static signal in arterial spin tagging (ASSIST). Magn Reson Med 2000;44(1):92–100.

33. Kim T, Kim SG. Quantitative MRI of cerebral arterial blood volume. Open Neuroimaging J 2011;5:136–145.